Experimental Comparison of Model Predictive Control and Cascaded Control of the Modular Multilevel Converter

Jan Böcker, Benjamin Freudenberg, Andrew The, and Sibylle Dieckerhoff, *Member, IEEE*

***Abstract*—This paper evaluates two different concepts for the control of the modular multilevel converter (MMC). Generally aiming at medium voltage applications, the considered MMC topology has a low number of submodules, and a pulse-width modulation (PWM) scheme is applied. A model predictive control (MPC) algorithm is developed and experimentally compared to a cascaded control scheme based on conventional PI controllers, which has been proposed by Hagiwara and Akagi. Steady-state and dynamic system performance as well as computational power requirements are discussed. The basis for the comparison is a scaled converter test bench operating from 560-V dc voltage.**

***Index Terms*—Circulating current control, model predictive control (MPC), modular multilevel converter (MMC), voltage source converter.**

I. Introduction

THE modular multilevel converter (MMC) was introduced in [1]. Due to its modular design, the topology is especially well suited for high voltage applications like high voltage direct current–voltage source converters (HVDC-VSC). For this specific application, commercial MMCs have been built using a medium to high number of half- or full-bridge submodule converters connected in series [2], [3]. These converters generate numerous voltage levels; therefore, they can operate at very low switching frequencies improving converter efficiency while at the same time achieving a low harmonic content in the output voltage.

The MMC is also considered feasible for medium voltage applications [4], [5]. In this case, the converter usually has a low number of submodules, thus a higher switching frequency is needed to increase the quality of the output voltage [6]. PWM schemes are generally applied to generate the switching signals. To achieve high dynamics and stable operation of the converter, a controller has to consider the inner dynamics of the MMC [7], [8].

Control concepts that include controlling of the circulating current and balancing of the capacitor voltages have been introduced in [9]–[11]. These concepts are based on conventional PI-controllers. Hagiwara and Akagi [9] proposes a concept that is specifically designed and experimentally tested for a MMC with a low number of submodules. The approach achieves a proper balancing of the capacitor voltages and damping of the ac part of the circulating current. However, since the circulating current is controlled via the sum of capacitor voltages within a phase leg, it cannot be directly manipulated with this control scheme. Other concepts according to [10], [11] transform the circulating current into a rotating dq-coordinate system and control the d- and q-components of the current separately. The reference values are provided by an outer control loop, alternatively, they may also be set to zero. Another control method using resonant controllers which affect the circulating current in the same manner is introduced in [12].

Different from these concepts, model predictive control (MPC) schemes allow us to directly influence several system variables simultaneously. Actually, MPC is gaining increased attention in power electronics, especially concerning its application to the control of multilevel converters, [13]–[16]. In contrast to the classic PI-controller-based concepts, MPC schemes do not need a modulator, since the switching states are directly set by the controller. MPC promises some significant advantages for converter control, including:

1) optimal control according to an optimization criterion;
2) dead time compensation;
3) consideration of nonlinear system behavior;
4) easy control of multiple variables;
5) limitation of controlled variables.

Hence, MPC is an attractive approach for the control of the MMC due to the converters high number of (partially coupled) system variables. However, a drawback of this concept is the relatively high computational hardware requirement in order to calculate the optimization problem online.

In this paper, a controller for the MMC is developed which is based on the finite control step MPC introduced in [17]. The focus of this paper lies on the practical implementation of the MPC. Therefore, a scaled test bench with a low number of submodules has been built and is used to verify the functionality of the developed MPC algorithm. In order to assess the MPC performance in comparison to a classic control approach based on cascaded PI-controllers, exemplarily the control scheme prosed in [9] is chosen and also implemented in the test bench. Experiments on steady state and dynamic performance are conducted for both control schemes and the results are compared.

The paper is structured as follows. After a brief summary of the MMC, the MPC algorithm is derived. Then, the control

Manuscript received September 30, 2013; revised January 27, 2014; accepted February 20, 2014. Date of publication March 3, 2014; date of current version August 26, 2014. Recommended for publication by Associate Editor M. (Guest EIC MMC) A. Perez.

The authors are with the Department of Power Electronics, Technische Universität Berlin, 10587 Berlin, Germany (e-mail: jan.boecker@tu-berlin.de; benjamin.freudenberg@tu-berlin.de; andrew.the@tu-berlin.de; sibylle.dieckerhoff@tu-berlin.de).

Digital Object Identifier 10.1109/TPEL.2014.2309438

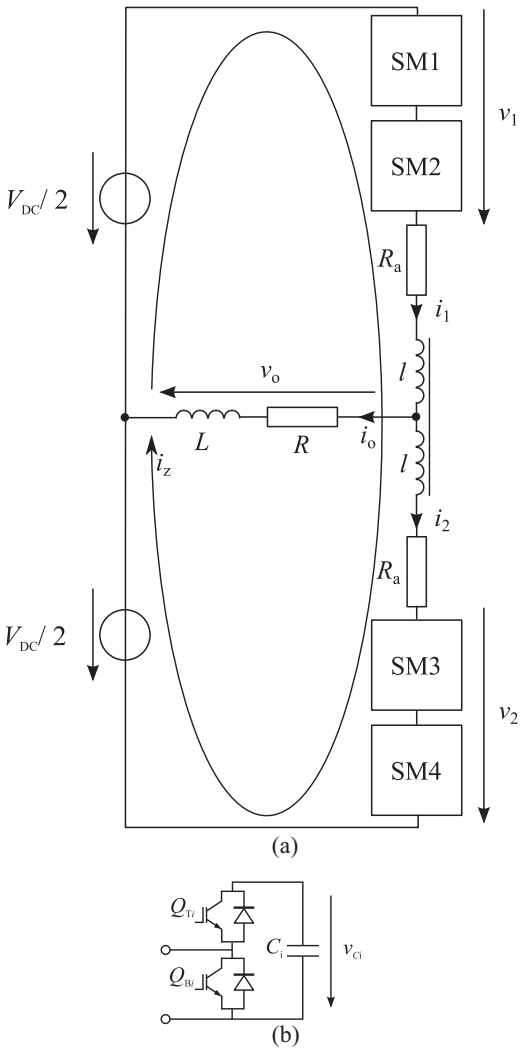

Fig. 1. Structure of a single phase MMC: (a) phase of MMC, (b) half-bridge submodule.

concept according to [9] is reviewed and adapted to our system. Finally, exemplary experimental results are discussed comparing the two concepts.

II. MMC Topology

A MMC phase leg consists of two MMC arms. Each arm has N submodules connected in series and an arm impedance, as shown in Fig. 1(a) for a single-phase configuration and $N = 2$. The submodules can be implemented as half-bridge, full-bridge or any VSC configuration. In this investigation, the half-bridge configuration is used to limit the complexity of the MPC [see Fig. 1(b)]. Depending on the state of the active switches, the capacitor C_i can be inserted into the MMC arm ($Q_{\mathrm{T}i}$ ON, $Q_{\mathrm{B}i}$ OFF) or bypassed ($Q_{\mathrm{T}i}$ off, $Q_{\mathrm{B}i}$ on) independently. Each capacitor is ideally charged to V_{DC}/N. Thus, the series connected N submodules of one arm can be described as a controlled voltage source. In a single-phase converter, we have the internal voltages v_1 and v_2. The quality of the generated internal voltage depends on the number of connected submodules and the deviation of the capacitor voltages caused by charging/discharging of the capacitors during converter operation. The latter implies that the capacitor voltages need to stay in balance to avoid distortion of the inner voltages and the output voltage. Neglecting the arm resistances and inductances, the output voltage follows the equation:

$$v_{\mathrm{o}} = \frac{v_2 - v_1}{2}. \tag{1}$$

The output current flowing through the load is calculated as

$$i_{\mathrm{o}} = \frac{v_{\mathrm{o}}}{Z_{\mathrm{load}}} = i_1 - i_2. \tag{2}$$

Different from a conventional converter, in which the current is delivered either from the upper or the lower arm, both MMC arms of a phase leg always carry half of the output current. In addition to the output current (noncirculating part) i_{o}, a current called the circulating current i_{z} is present. This current consists of a dc part that describes the energy transfer from the dc link to the submodule capacitors, and an ac part that is caused by the unavoidable deviation in capacitor voltages. If the sum of inserted voltages is lower than the dc link voltage V_{DC}, the dc link will deliver a positive circulating current i_{z} to compensate the voltage difference. Otherwise, the circulating currents flow from the phase leg to the dc link, resulting in a negative value. The circulating current can be defined as

$$i_{\mathrm{z}} = \frac{i_1 + i_2}{2}. \tag{3}$$

Because the circulating current rises the rms value of the arm currents according to the following equation:

$$I_{1,2} = \sqrt{I_{\mathrm{z}}^2 + \frac{I_{\mathrm{o}}^2}{4}} \tag{4}$$

it is necessary to control i_{z} to reduce arm losses. Furthermore, resonances may occur in the converter which need to be suppressed.

Internal dynamic parameters of the MMC such as the capacitor voltages and the circulating current need to be controlled in order to achieve internal stability of the converter. Both considered control concepts—the cascaded control and the MPC—take this into account. Generally, there will also be a system control for the outer dynamic parameters. In this paper, we have implemented a control of the output current to compare the dynamic performance of both control concepts. A relatively high switching frequency is applied so that only small ripples are visible in the output current. Both control concepts will be explained in the next two sections.

III. Model Predictive Control

MPC uses a model of a system to predict its future behavior. This prediction is used to calculate the actuation signals that deliver an optimal behavior of the controlled variables. An optimization criterion defined as a cost function ensures that the desired behavior is achieved.

In order to solve the optimization problem online in a reasonable time frame, it is necessary to implement limitations such as time discretization, model linearization, and reduction

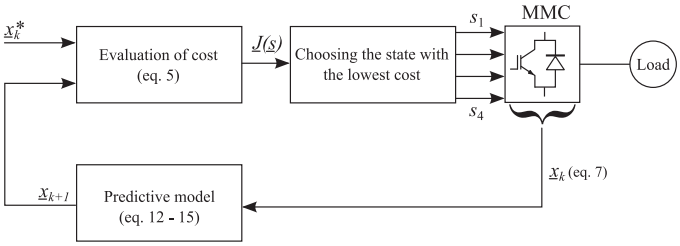

Fig. 2. Principle of MPC according to [17].

of the prediction horizon. However, there exist a lot of possibilities to reduce the complexity of the optimization problem, thus there are many classes of predictive controllers. Cortés *et al.* [18] give an overview of different predictive controllers for converter systems.

In this paper, a MPC for the MMC with strict limitations is developed, namely time discretization and one-step prediction. This control is based on the algorithm that is presented by J. Rodriguez and P. Cortes in [17] and [13]. Further MPC algorithms for the MMC are published in [19], [14], and [15].

A. Time Discrete MPC

The implemented control scheme works with a constant sample frequency f_s. The actuating variables are the switching signals of the half bridges; no modulator is needed. Hence, switching is only possible in discrete time steps. Fig. 2 shows the closed loop control of the converter system. The predictive control algorithm is straightforward and includes the following steps [17]:

1) Predict the values of the controlled variables for all possible switching states for the next time step,
2) evaluate the cost function for each prediction, and
3) select the switching state that minimizes the cost function.

For the considered single-phase converter with two submodules per arm, the controller has to evaluate $2^{2N} = 16$ switching states in one sample period. In case of a three-phase system, the controller needs to calculate $2^{3\cdot 2N} = 4096$ switching states. Generally, the calculating time rises exponentially with the number of submodules. Therefore, additional limitations will be needed if the system becomes more complex.

In the practical implementation, an additional dead time is introduced because of the calculating time. The calculation is done within one sample period, so the dead time is T_s. This dead time will impair the performance visibly. However, it is very simple to compensate this dead time through an additional prediction of one time step using the actual switching state. All experiments are conducted with dead time compensation.

B. Cost Function

The cost function has to define the optimal values of the controlled variables. In our case, the cost function evaluates only the next sample period $(k+1)$, since the prediction is not done for more time steps. With respect to the calculating speed, the cost function J should be of low complexity but fulfill all requirements defined in Section II. This results in the function

$$J = \lambda_1 |i_{o,k+1} - i_{o,k}^*| + \lambda_2 |i_{\mathrm{z},k+1} - i_{\mathrm{z},k}^*| + \lambda_3 \sum_{i=1}^{2N} (v_{Ci,k+1} - v_{C,k}^*)^2 + \lambda_4 n_{s,k+1}. \quad (5)$$

The character "$*$" denotes reference values. The parameters λ_1, λ_2, λ_3, and λ_4 are weighting factors that can be used to set the priority of a controlled variable. n_s is the quantity of switching processes that were performed between the sample periods k and $k+1$ in order to reach the new switching state. The calculation of this quantity results in

$$n_s = 2 \sum_{i=1}^{2N} |s_{i,k} - s_{i,k+1}| \quad (6)$$

where $s_1, \ldots, s_2 N \in \{0; 1\}$ are the switching signals of each submodule. This term in the cost function is used to reduce the switching frequency without changing the sample frequency. The switching of both IGBTs in a submodule is considered in (6), thus the factor 2. The deviation of the capacitor voltages from their reference is weighted with a quadratic function. Because of this nonlinear function, the term can reach two requirements, controlling the mean value of all voltages and balancing of the voltages in one arm.

The development of the cost function is a problem of the MPC: it is quite simple to find a cost function which shows adequate control results, but it is very difficult to analyze the choice of the function and the influence of the individual weighting factors on the results and to optimize them. Some information about designing cost function and the weighting factors is given in [13] and [20]. The optimization of the weighting factors for the MMC, however, is very complex, because the controlled variables are dependent on each other. In this paper, starting with reasonable assumptions, the factors are selected based on a simulation analysis varying the factors. Obviously, this procedure is not really efficient if the cost function contains a high number of coupled variables.

C. System Model

A good system model is crucial for the performance of the MPC. The accuracy of the model directly influences the control error, and the calculation speed mainly depends on the model complexity.

The single-phase MMC is completely described by the following state vector $\underline{x}$ with the arm currents and the capacitor voltages as state variables:

$$\underline{x} = \begin{bmatrix} i_1 \\ i_2 \\ v_{\mathrm{C1}} \\ \vdots \\ v_{\mathrm{C2N}} \end{bmatrix}. \quad (7)$$

To calculate the arm currents i_1 and i_2, generally the following differential equations can be set up:

$$\frac{V_{\mathrm{DC}}}{2} = v_1 + R(i_1 - i_2) + l\frac{di_1}{dt} + L\frac{d(i_1 - i_2)}{dt} + i_1 R_a \quad (8)$$

$$V_{\mathrm{DC}} = v_1 + v_2 + l\left(\frac{di_1}{dt} + \frac{di_2}{dt}\right) + R_a(i_1 + i_2). \quad (9)$$

However, these equations are not valid for coupled arm inductances l, which are used in our converter. Assuming that the load current i_o splits up symmetrically into the two arm currents, this results in

$$i_1 - i_z = -i_2 + i_z = i_o/2 \quad (10)$$

according to (3) and (4). Hence, a modified load inductance

$$\tilde{L} = L - l/2 \quad (11)$$

can be defined which includes the coupling effect.

Combining (8), (9), and (11) results in the state space equation

$$(2L + l)\begin{bmatrix}\frac{di_1}{dt}\\ \frac{di_2}{dt}\end{bmatrix} = \begin{bmatrix} V_{\mathrm{DC}}\left(\frac{1}{2} + \frac{\tilde{L}}{l}\right)\\ V_{\mathrm{DC}}\left(\frac{1}{2} + \frac{\tilde{L}}{l}\right)\end{bmatrix} + \begin{bmatrix} -R - R_a\left(1 + \frac{\tilde{L}}{l}\right) & R - R_a\left(1 + \frac{\tilde{L}}{l}\right)\\ R - R_a\left(1 + \frac{\tilde{L}}{l}\right) & -R - R_a\left(1 + \frac{\tilde{L}}{l}\right)\end{bmatrix} \cdot \begin{bmatrix} i_1\\ i_2\end{bmatrix} + \begin{bmatrix} -1 - \frac{\tilde{L}}{l} & -\frac{\tilde{L}}{l}\\ -\frac{\tilde{L}}{l} & -1 - \frac{\tilde{L}}{l}\end{bmatrix} \cdot \begin{bmatrix} v_1\\ v_2\end{bmatrix}. \quad (12)$$

The voltages v_1 and v_2 are defined by the switching function $\underline{s} \in \{0;1\}^4$

$$v_1 = s_1 \cdot v_{\mathrm{C1}} + s_2 \cdot v_{\mathrm{C2}} \quad (13)$$

$$v_2 = s_3 \cdot v_{\mathrm{C3}} + s_4 \cdot v_{\mathrm{C4}}. \quad (14)$$

The capacitor voltages are described by the following equation:

$$\frac{dv_{\mathrm{Ci}}}{dt} = \begin{cases} s_i \cdot \dfrac{i_1}{C} & \text{with } i \le 2\\ s_i \cdot \dfrac{i_2}{C} & \text{with } i > 2.\end{cases} \quad (15)$$

To reduce computation time, the simple Euler forward method which results in

$$\left.\frac{d\underline{x}(t)}{dt}\right|_{kT_s} \approx \frac{\underline{x}_{k+1} - \underline{x}_k}{T_s} = f(\underline{x}_k) \quad (16)$$

is applied to discretize (12) with the sampling period T_s.

Since the arm currents are changing very fast, the capacitor voltages need to be predicted with a higher accuracy. Therefore, (15) is discretized according to

$$\left.\frac{d\underline{x}(t)}{dt}\right|_{kT_s} \approx \frac{\underline{x}_{k+1} - \underline{x}_k}{T_s} = \frac{f(\underline{x}_k) + f(\underline{x}_{k+1})}{2}. \quad (17)$$

IV. Cascaded Control Concept Based on PI Controllers

Up to now, several different control concepts based on PI-controllers have been presented for the control of the inner and outer dynamics of the MMC. In [10] and [11], the circulating current i_z is manipulated by transforming this current into rotating dq-reference frames and controlling its d- and q-components separately with PI-controllers. In this way, it is possible to control the dominant ac parts of the circulating current, whether it is the first harmonic with the fundamental frequency or the second harmonic. The main idea given in [10] is to suppress the ac part of the circulating current which oscillates with twice the fundamental frequency f_2. Therefore, the circulating current is transformed into dq-coordinates rotating with f_2, and a reference value of zero is given for both d- and q-components. The concept in [11] is principally based on the idea of [10]. It extends the control structure with an additional dq-system rotating with fundamental frequency. The circulating current which is divided into a fundamental and twice the fundamental frequency part is used to balance the energy distribution in the MMC arms. The reference value for the circulating current suppressing controller is generated by the energy controller which controls the sum of energies stored in one phase leg and the difference of energies stored between the arms of one phase leg. The ac part of the circulating current is, thus, not suppressed to zero. A different control concept is described in [9], which does not rely on the transformation in rotating coordinate systems. Here, the control structure can also be divided into two different parts. One part controls the circulating current through controlling the average value of all submodule voltages, the other part balances the submodule voltages. This control structure has been chosen for the practical comparison with the MPC due to the fact that it can be realized in single and three-phase converter systems. Because of its high number of possible switching states, described in Section III, and the present controller hardware limitation in our experimental setup, the MPC is implemented for a single-phase MMC, see Section V.

For a comparison of this approach with the MPC of Section III, in addition to the internal variables of the MMC also the output current needs to be controlled. The whole control structure is summarized in Fig. 3.

A. Control of the Output Current

The output current i_o has to follow an ideal sine wave reference current. The control loop consists of a PI controller, an ohmic-inductive load (R, L), and a dead time which results from the generation of the switching signals and the sampling of the measured signals. For stable and good system performance, the control parameters are chosen using the modulus optimum. They are summarized in Table II.

B. Control of Internal Variables

The control of the internal variables is based on the concept of H. Hagiwara and H. Akagi which was published in 2009 [9]. The concept combines three different tasks, see Section II, and

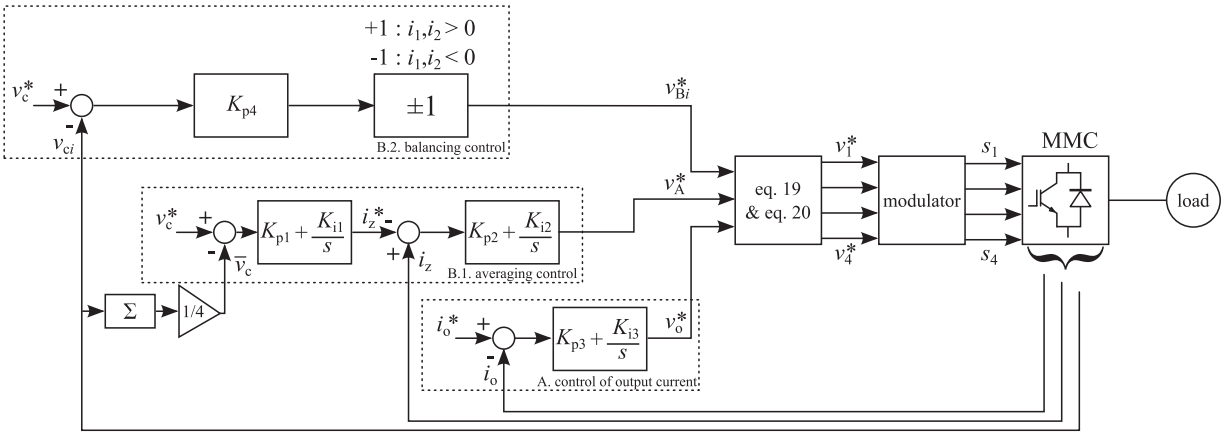

Fig. 3. Structure of the cascaded control loop according to [9].

is split into two different control loops named *averaging control* and *balancing control* [9].

1) Averaging Control: The averaging control consists of a cascaded structure: the inner loop controls the circulating current i_z, and the outer loop controls the average value of the submodule voltages given by

$$\bar{v}_C = \frac{1}{4}\sum_{i=1}^{4} v_{Ci}. \tag{18}$$

Forming a part of the total output reference voltage for the modulator, the algorithm yields the reference voltage v_A^*.

The control parameters for the inner loop are designed based on a system model including a dead time, caused by the sampling time, and an ohmic-inductive element which consists of the arm resistor R_a and the arm inductance l, see Fig. 1. The plant for the outer voltage loop includes the closed circulating current control loop and the effective capacitance of the submodules. Specifically, the time constant of the voltage controller has to be selected so that a second-order harmonic in the submodule voltages is allowed, thus preventing extremely high current reference values i_z^*. The chosen parameters are also given in Table II.

2) Balancing Control: The balancing of the submodule voltages is achieved using a proportional controller. The output of this controller is multiplied by ± 1 depending on the sign of the arm current as depicted in Fig. 3. With the final control output v_{Bi}^*, a small value is added to or subtracted from the reference voltage. In consequence, the on- or off-time of the associated submodule is changed.

C. Combining the Control Loops

The switching signals for each submodule are derived from individual modulators which operate with a carrier-based PWM. The triangular carrier signals change between zero and $V_{DC}/2$. To obtain the reference value for the output voltage that is fed to each modulator, the three results from the different control loops have to be summarized for each submodule separately. For the upper submodules $(i = 1, 2)$, the reference value can be calculated to

$$v_i = v_A^* + v_{Bi}^* - v_o^*/2 + V_{DC}/4 \tag{19}$$

and for the lower submodules $(i = 3, 4)$

$$v_i = v_A^* + v_{Bi}^* + v_o^*/2 + V_{DC}/4. \tag{20}$$

The reason for adding half of the reference value of the output voltage and one-fourth of the dc-link voltage are the already mentioned individual modulators for each submodule. In our case, there are four different triangular carrier signals which are phase shifted to each other. The carrier signals for the upper arm are phase-shifted by 180° to each other. The carrier signals for the lower arm are also phase-shifted by 180° to each other, but they are phase-shifted by 90° in comparison to the upper arm carriers.

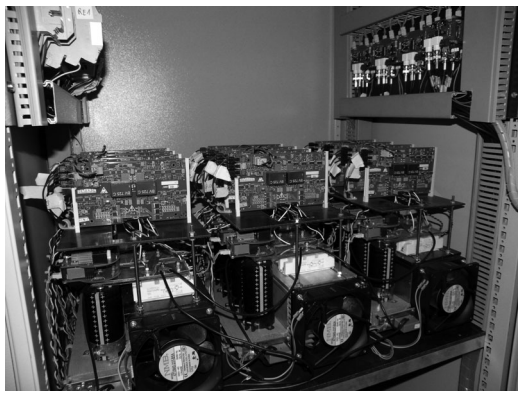

Fig. 4. Three-phase MMC test bench.

V. Experimental Results

A. Experimental Setup

The two concurring control concepts are investigated using a scaled converter test bench. The test bench consists of a three-phase MMC (see Fig. 4) with a basic number of $N = 2$ submodules per arm, a rated power of 12 kW and a dc link voltage of 560 V. For this investigation, we were restricted to a single-phase configuration in order to match the complexity of the MPC with

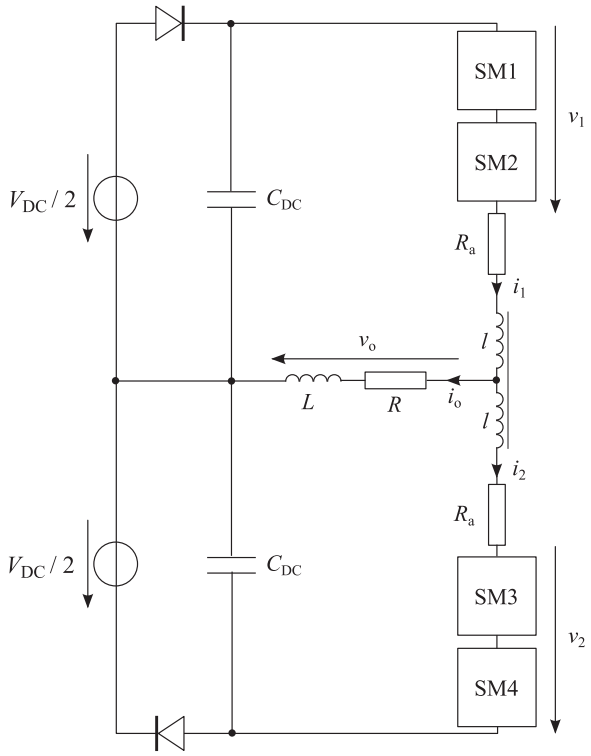

Fig. 5. Experimental setup for the single phase circuit.

TABLE I
TEST-BENCH PARAMETERS

Parameter	Symbol	Value
DC link voltage	V_{dc}	560 V
No. of submodule per arm	N	2
Nominal submodule voltage	V_{Ci}	280 V
Submodule capacitor	C_i	2.2 mF
Arm resistance	R_{a}	400 mΩ
Arm inductance	l	1.5 mH
Load resistance	R	43 Ω
Load inductance	L	4 mH

our latest control system. The remaining two of the three phase legs are used as the dc link to provide a constant dc voltage for the single-phase converter, as shown in Fig. 5. The diodes installed between the dc link capacitors and the dc sources are a safety measure ensuring that no current flows back to the dc sources. In the presented experiments, the converter operates with a dc link voltage of 560 V and a peak load current of 5 A supplying a passive ohmic-inductive load. The setup parameters are summarized in Table I.

B. Comparison Under Steady-State Conditions

For the evaluation of the steady-state performance, the converter operates with a peak output current of 5 A. The scaled setup is intended to investigate medium voltage applications, therefore the switching frequency of a submodule is set to $f_{\mathrm{c}} = 1$ kHz. The MPC parameters which are summarized in Table II are chosen so that a comparable average switching frequency $\bar{f}_{\mathrm{sw}} = 1.08$ kHz of one submodule is achieved. This frequency is

TABLE II
CONTROLLER PARAMETERS

Conventional		MPC	
Parameter	Value	Parameter	Value
K_{p1}	$0.5\,\frac{\mathrm{A}}{\mathrm{V}}$	λ_1	$1\,\frac{1}{\mathrm{A}}$
K_{i1}	$80\,\frac{\mathrm{A}}{\mathrm{Vs}}$	λ_2	$0.067\,\frac{1}{\mathrm{A}}$
K_{p2}	$1\,\frac{\mathrm{V}}{\mathrm{A}}$	λ_3	$0.033\,\frac{1}{\mathrm{V}^2}$
K_{i2}	$300\,\frac{\mathrm{V}}{\mathrm{As}}$	λ_4	0.06
K_{p3}	$13.3\,\frac{\mathrm{V}}{\mathrm{A}}$	f_{s}	8 kHz
K_{i3}	$53\,333.2\,\frac{\mathrm{V}}{\mathrm{As}}$	$\bar{f}_{\mathrm{sw}}$	1.08 kHz
K_{p4}	0.35		
f_{c}	1 kHz		
f_{s}	4 kHz		

comparable to the carrier frequency f_c of the conventional modulator which also describes the average switching frequency of one submodule. Comparable f_c and $\bar{f}_{\mathrm{sw}}$ result in similar output waveforms. The steady-state results are shown in Figs. 6 and 7.

With the $N = 2$ submodules per arm, both control schemes generate a five level output voltage. Compared to the cascaded control from Section IV, the pulse pattern of the MPC shows an irregular switching frequency. One cause of this irregularity is the missing modulator in the MPC; another cause is the limited sampling time of the MPC, which also limits the smallest interval, in which a state change of submodules can occur. This sampling time defines the switching instances of the MPC.

The output currents show similar deviations from an ideal sine wave. The analysis of the distortion factors for the considered point of operation results in $THD_{\mathrm{MPC}} = 9.8\%$ and $THD_{\mathrm{conv.}} = 8.7\%$. In this case, the cascaded control shows a better result compared to the MPC. But it is important to note that the implemented MPC algorithm is more subject to measurement disturbances, since the sampling of the analog signals occurs in those instances where the submodules are switching.

The circulating current exhibits a very high ripple in both control concepts. Those switching states that result in an intermediate output voltage level, i.e., $v_o = V_{\mathrm{DC}}/4$, cause a higher voltage at the arm inductances than other switching states. These voltages, however, are needed to control the circulating current. In spite of the high ripple, both circulating currents show a good stability. Applying MPC, the ripple is smaller and more irregular in some points compared to the cascaded control.

Both control concepts cause a peak-to-peak ripple that is as high as the output current. This ripple produces additional losses in the semiconductors and can be reduced by increasing the switching frequency or choosing a higher arm inductance, which in turn lead to higher switching losses or additional costs and weight. Another option to reduce the ripple is to increase the number of submodules while maintaining the same dc link voltage level. The relative voltages of the arm inductors decrease due to the lower submodule voltage, thus decreasing the current ripple.

Balancing of the submodule voltages is achieved with both algorithms but with different quality. It should be noted that very high frequency components in the measured waveforms of the submodule voltages are filtered via software, see Figs. 6 and 7.

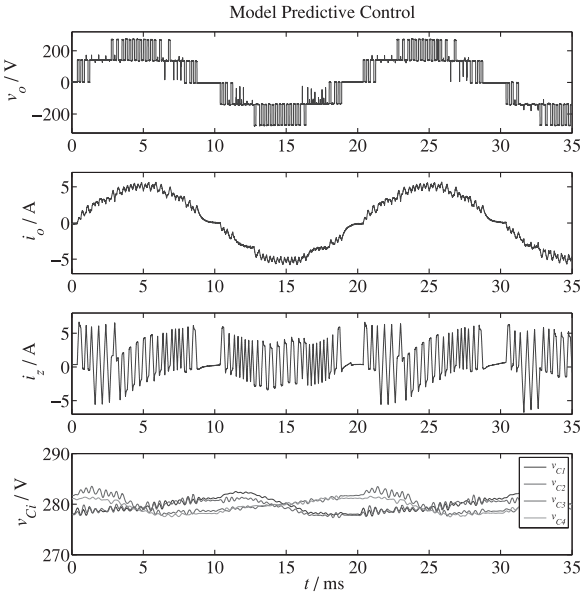

Fig. 6. Steady-state results of the model predicive control.

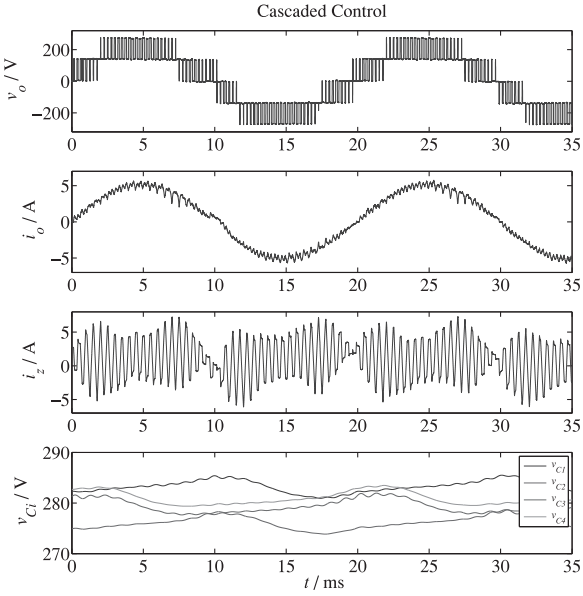

Fig. 7. Steady-state results of the cascaded control.

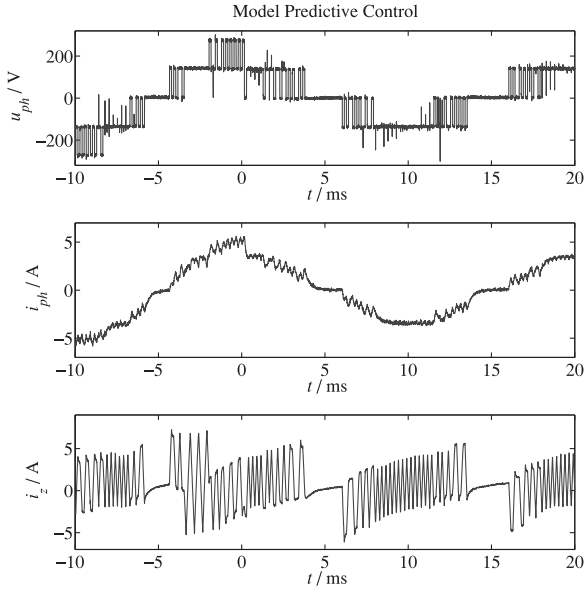

Fig. 8. Dynamic performance of the MPC.

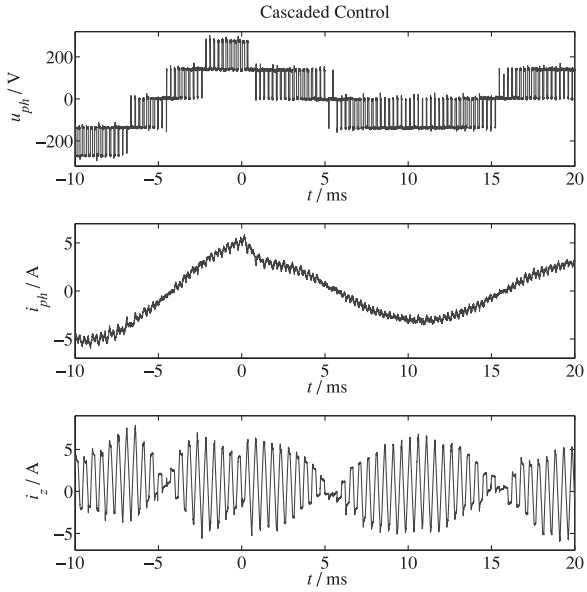

Fig. 9. Dynamic performance of the cascaded control.

As depicted in the bottom diagram of Fig. 6, the MPC shows good voltage balancing of the submodules in each arm. The voltages of both arms in the phase leg are also well balanced. The balancing achieved with the cascaded control algorithm is also acceptable, but the voltages of the upper arm (blue and green curves in the bottom diagram of Fig. 7) show a significant difference in the dc level compared to the lower submodule voltages (red and light blue curves). This problem is caused by the dead time of the controller and could be canceled out by increasing the sampling frequency. With the MPC, better results are obtained because of the implemented dead time compensation.

The MPC calculation time for all 16 switching states of the considered single-phase converter is about 40 μs. In case of a three-phase configuration, the number of possible states rises to 4096 states, which exceeds the calculation speed of our latest control system. On the other hand, the calculation time of the cascaded controller would increase only by a factor of three for a three-phase system. The required computational power is one severe disadvantage of the MPC.

C. Comparison of Dynamic Behavior

In this section, the dynamic performance of the controllers is discussed. Exemplarily, a peak load current step from 5 to 3 A is applied. In this way, the performance of the load current control and the circulating current control can be assessed. The circulating current has to change very fast in order to balance

the input and output power. In Figs. 8 and 9, the output current step is applied at the time $t = 0$.

Fig. 8 shows the measured output voltage, output current, and circulating current in response to the load step using MPC. The plots indicate a high stability of the system as there is no additional ringing on the circulating current i_{Z}. The dynamics of the output current i_{o} is very high, which can be recognized from the steep slope at $t = 0$. The current changes very fast to the new reference value without any overshoot.

Fig. 9 depicts the step response applying the cascaded control loop. The system also reacts stably on the current step. However, the dynamics of the output current i_0 is lower compared to the MPC. This is due to the fact that the dynamics of the cascaded control loop is limited by the dead time caused by the calculation time and the discretization of the reference value. In our implementation, the dead time is about one and a half sample period, with a sample frequency f_{s} of $4 \cdot f_{\mathrm{c}} = 4$ kHz. The model predictive controller compensates the calculation dead time, and the prediction reduces the overshoot. In fact, the overall dynamic performance of the MPC is superior to the cascaded control. The high dynamics is a significant advantage of the MPC.

VI. Conclusion

In this paper, a MPC algorithm is developed for the control of a MMC with a low number of submodules. This concept is experimentally compared to a cascaded control scheme based on conventional PI controllers. Both considered concepts give good results controlling the internal variables and the output current of the MMC. Since the structure of the MPC is quite simple, it is remarkable that a comparable steady-state performance can be easily achieved with this approach. The dynamic performance of the MPC controlled converter is even superior to the considered PI control, due to the prediction and hence knowledge of the future converter behavior. A significant disadvantage of the implemented MPC algorithm is the required processing power, which rises exponentially with the number of switching states. Without additional restrictions, which will compromise control performance, the concept is not feasible for multilevel converters with a huge number of possible switching states.

References

[1] A. Lesnicar and R. Marquardt, "An innovative modular multilevel converter topology suitable for a wide power range," in *Proc. IEEE Power Tech. Conf.*, 2003, vol. 3, p. 6.

[2] H. Gambach, M. Wahle, and D. Schuster, "Self-commutated converters (MMC) for the connection of offshore windfarms," *Bauelemente der Leistungselektronik und ihre Anwendungen ETG-Fachtagung Bad Nauheim*, ETG-Fachbericht, 13–14 Apr. 2011, vol. 128, pp. 131–140.

[3] B. Jacobson, P. Karlsson, G. Asplund, L. Harnefors, and T. Jonnson, "VSC-HVDC transmission with cascaded two-level converters," presented at the *Council on Large Electric Systems (CIGRE)*, Paris, France, 2010.

[4] M. Hiller, D. Krug, R. Sommer, and S. Rohner, "A new highly modular medium voltage converter topology for industrial drive applications," in *Proc. 13th Eur. Conf. Power Electron. Appl.*, 2009, pp. 1–10.

[5] A. Korn, M. Winkelnkemper, P. Steimer, and J. Kolar, "Direct modular multi-level converter for gearless low-speed drives," in *Proc. 14th Eur. Conf. Power Electron. Appl.*, 2011, pp. 1–7.

[6] S. Rohner, S. Bernet, M. Hiller, and R. Sommer, "Modulation, losses, and semiconductor requirements of modular multilevel converters," *IEEE Trans. Ind. Electron.*, vol. 57, no. 8, pp. 2633–2642, Aug. 2010.

[7] A. Antonopoulos, L. Angquist, and H.-P. Nee, "On dynamics and voltage control of the modular multilevel converter," in *Proc. 13th Eur. Conf. Power Electron. Appl.*, 2009, pp. 1–10.

[8] K. Ilves, A. Antonopoulos, S. Norrga, and H.-P. Nee, "Steady-state analysis of interaction between harmonic components of arm and line quantities of modular multilevel converters," *IEEE Trans. Power Electron.*, vol. 27, no. 1, pp. 57–68, Jan. 2012.

[9] M. Hagiwara and H. Akagi, "Control and experiment of pulsewidth-modulated modular multilevel converters," *IEEE Trans. Power Electron.*, vol. 24, no. 7, pp. 1737–1746, Jul. 2009.

[10] Q. Tu, Z. Xu, and J. Zhang, "Circulating current suppressing controller in modular multilevel converter," in *Proc. IEEE IECON—36th Annu. Conf. Ind. Electron. Soc.*, 2010, pp. 3198–3202.

[11] G. Bergna, E. Berne, P. Egrot, P. Lefranc, A. Arzande, J.-C. Vannier, and M. Molinas, "An energy-based controller for HVDC modular multilevel converter in decoupled double synchronous reference frame for voltage oscillation reduction," *IEEE Trans. Ind. Electron.*, vol. 60, no. 6, pp. 2360–2371, Jun. 2013.

[12] Z. Li, P. Wang, Z. Chu, H. Zhu, Y. Luo, and Y. Li, "An inner current suppressing method for modular multilevel converters," *IEEE Trans. Power Electron.*, vol. 28, no. 11, pp. 4873–4879, Nov. 2013.

[13] J. Rodriguez and P. Cortes, *Predictive Control of Power Converters and Electrical Drives*. New York, NY, USA: Wiley, 2012.

[14] J. Qin and M. Saeedifard, "Predictive control of a modular multilevel converter for a back-to-back HVDC system," *IEEE Trans. Power Del.*, vol. 27, no. 3, pp. 1538–1547, Jul. 2012.

[15] B. S. Riar, T. Geyer, and U. K. Madawala, "Model predictive direct current control of modular multi-level converters," in *Proc. IEEE Int. Conf. Ind. Technol.*, 2013, pp. 582–587.

[16] T. Geyer, "Model predictive direct current control for multi-level converters," in *Proc. IEEE Energy Convers. Congr. Expo.*, 2010, pp. 4305–4312.

[17] S. Kouro, P. Cortés, R. Vargas, U. Ammann, and J. Rodríguez, "Model predictive control—A simple and powerful method to control power converters," *IEEE Trans. Ind. Electron.*, vol. 56, no. 6, pp. 1826–1838, Jun. 2009.

[18] P. Cortés, M. P. Kazmierkowski, R. M. Kennel, D. Quevedo, and J. Rodríguez, "Predictive control in power electronics and drives," *IEEE Trans. Ind. Electron.*, vol. 55, no. 12, pp. 4312–4324, Dec. 2008.

[19] M. A. Perez, J. Rodríguez, E. J. Fuentes, and F. Kammerer, "Predictive control of AC-AC modular multilevel converters," *IEEE Trans. Ind. Electron.*, vol. 59, no. 7, pp. 2832–2839, Jul. 2012.

[20] P. Cortes, S. Kouro, B. La Rocca, R. Vargas, J. Rodriguez, J. Leon, S. Vazquez, and L. Franquelo, "Guidelines for weighting factors design in model predictive control of power converters and drives," in *Proc. IEEE Int. Conf. Ind. Technol.*, 2009, pp. 1–7.

Jan Böcker was born in Berlin, Germany, in 1988. He received the M.Sc. degree in electrical engineering from the Technische Universität Berlin, Berlin, Germany, in 2013. He is currently working toward the Ph.D. degree at the Power Electronics Group, Technische Universität Berlin.

His research interests include multilevel topologies, model predictive control, and wide bandgap semiconductors.

Benjamin Freudenberg was born in Berlin, Germany, in 1987. He received the M.Sc. degree in electrical engineering from the Technische Universität Berlin, Berlin, Germany, in 2013. Since 2013, he has been working toward the Ph.D. degree at the Power Electronics Group, Technische Universität Berlin.

His research interests include multilevel converters and its control methods.

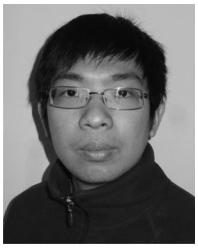

Andrew The was born in Surakarta, Indonesia, in 1985. He received the M.Sc. degree in electrical engineering from the Berlin Institute of Technology/Technische Universität Berlin, Berlin, Germany, in 2011. Since 2011, he has been working toward the Ph.D. degree at the Power Electronics Group, Technische Universität Berlin.

His interests include multilevel topologies, modular multilevel converters for HVDC and medium voltage applications and its control methods.

Sibylle Dieckerhoff (M'04) received the Dipl.-Ing. and Dr.-Ing. degrees in electrical engineering from RWTH Aachen, Aachen, Germany, in 1997 and 2003, respectively.

From 1997 to 2002, she was a Research Associate with the Institute for Power Electronics and Electrical Drives, RWTH Aachen and with DaimlerChrysler Research and Technology, Berlin. Following her Ph.D. degree in 2003, she worked as a Development Engineer at Siemens AG, as a Senior Researcher at TU Berlin, and as a Professor at Beuth University of Applied Sciences, Berlin, before joining TU Berlin in 2010, where she is currently a Professor for Power Electronics.